Condensed Matter Physics, 2017, Vol. 20, No 2, 23705: 1–16
DOI: 10.5488/CMP.20.23705
http://www.icmp.lviv.ua/journal

CONDENSED MATTER PHYSICS

Interaction of NH_3 gas on α-MoO_3 nanostructures — a DFT investigation

V. Nagarajan, R. Chandiramouli*

School of Electrical and Electronics Engineering, Shanmugha Arts Science Technology and Research Academy (SASTRA) University, Tirumalaisamudram, Thanjavur, Tamil nadu — 613 401, India

Received February 21, 2017, in final form April 18, 2017

The structural stability, electronic properties and NH_3 adsorption properties of pristine, Ti, Zr and F substituted α-MoO_3 nanostructures are successfully studied using density functional theory with B3LYP/LanL2DZ basis set. The structural stability of α-MoO_3 nanostructures is discussed in terms of formation energy. The electronic properties of pristine, Ti, Zr and F incorporated α-MoO_3 nanostructures are discussed in terms of HOMO-LUMO gap, ionization potential and electron affinity. α-MoO_3 nanostructures can be fine-tuned with suitable substitution impurity to improve the adsorption characteristics of ammonia, which can be used to detect NH_3 in a mixed environment. The present work gives an insight into tailoring α-MoO_3 nanostructures for NH_3 detection.

Key words: *nanostructure, adsorption, NH_3, HOMO-LUMO gap, MoO_3*

PACS: *71.15.Mb*

1. Introduction

Ammonia (NH_3) is widely used in automobiles, food industry and agriculture in the form of fuel, antimicrobial agent and fertilizers [1]. The detection of NH_3 is a significant criterion due to its hazard. The exposure limit of ammonia is around 25 ppm, which is recommended by Occupational Safety and Health Administration (OSHA) [2]. There are several analytical techniques adopted to detect ammonia gas, which include the laser methods [3], electrochemical methods, optical methods [4] and mass spectrometry [5]. These techniques are time-consuming and also need sophisticated instruments. In this context, an inexpensive and real-time sensor is required to detect trace the amounts of ammonia at ppm level. Metal oxide semiconductor (MOS) thin films are extensively used for gas sensors as their resistivity changes upon interaction with toxic gas molecules [6, 7]. Moreover, MOS sensors are easy to fabricate, low cost and are uniform in performance among other types of gas sensors. Besides, the morphology such as rods, belts and wires in the micro-dimension and nano-dimension show a significant performance in MOS sensors. Furthermore, these types of nanostructured materials offer high surface-to-volume ratio, which leads to an enhanced performance in gas sensing [8–10].

Among various metal oxide semiconductors, molybdenum oxide (MoO_3) is an excellent candidate for electrochromic, catalytic and gas sensing applications. MoO_3 is n-type semiconductor with a wide band gap; the conductivity arises due to oxygen vacancies. The band gap of MoO_3 is found to be around 2.69–2.76 eV [11]. MoO_3 is also used as catalyst for the reduction of NO_x in the petroleum and chemical industry and oxidation of hydrocarbons [12–15]. Moreover, there are reports for enhancing the gas sensing properties of molybdenum oxide based device to detect LPG [16], CO [17, 18], NH_3 [13, 16, 19], H_2 [16, 17]. Furthermore, the synthesis of MoO_3 includes thermal evaporation [20], pulsed laser deposition [13], sol-gel [1, 21], electro-deposition [22] and chemical vapor deposition [23, 24].

MoO_3 exhibits in three polymorphic phases [25] namely stable orthorhombic α-MoO_3, meta-stable monoclinic β-MoO_3, hexagonal β-MoO_3. Kannan et al. [26] have reported the influence of the precursor

*Corresponding author

solution volume on the properties of spray deposited α-MoO_3 thin films. Martinez et al. [27] have studied the gas sensing properties of spray deposited MoO_3 thin films. Hussain et al. [28] have reported activated reactive evaporated MoO_3 thin films for gas sensor applications and they observed that α-MoO_3 are capable of sensing both CO and NH_3 gases at below 10 ppm of concentration in dry air. Density functional theory (DFT) is an efficient method for studying the interaction between compounds and adsorption characteristics of compounds [29–31]. Based on these aspects, literature survey was conducted using CrossRef metadata search and it is inferred that not much work was reported based on DFT methods to investigate the adsorption properties of NH_3 on α-MoO_3 nanostructures. The motivation behind the present work is to improve the NH_3 adsorption properties on α-MoO_3 nanostructures with the incorporation of dopants. The novel aspect of this work is to study the adsorption characteristics of NH_3 on α-MoO_3 nanostructures with the substitution of Ti, Zr and F as substitution impurities.

2. Computational methods

In the present work, Gaussian 09 package [32] is used to optimize the pristine, Ti, Zr and F substituted α-MoO_3 nanostructures. This package is also used to investigate the adsorption properties of NH_3 gas molecules on α-MoO_3 base material. The calculations were carried out for isolated MoO_3 base material with periodic boundary condition (PBC). Moreover, the atoms were fixed along the direction perpendicular to the molecular plane and allowed us to relax along the other planes. In the present work, DFT is utilized in accordance with Becke's three-parameter hybrid functional in combination with Lee-Yang-Parr correlation functional (B3LYP)/LanL2DZ basis set [33–36]. The selection of a suitable basis set is an important criterion for optimizing α-MoO_3 nanostructures. In our previous study we demonstrated a density functional theory with the use of all-electron basis sets, but methods including effective core potentials (ECPs) are good in reducing the computational cost. Furthermore, the efforts have been taken into account for measuring the performance of basis set in order to approximate the same set of density functional. Moreover, we used ECP basis set such as LanL2DZ (Los Alamos National Laboratory 2 Double-Zeta), which is more suitable for transition metals. Besides, utilization of all-electron basis sets for the remaining non-transition metal elements has become more popular in computational studies on transition metal containing materials. Further, the atomic number of molybdenum and oxygen is forty two and eight, respectively. In the present work, α-MoO_3 nanostructures are studied with the incorporation of impurities such as Ti, Zr and F. It is known that Ti and Zr belongs to group IVB and is 4th and 5th period, respectively. Thus, LanL2DZ effective core potential will be suitable for the optimization of α-MoO_3 nanostructures with impurities. In addition, LanL2DZ basis set is applicable for the elements such as H, Li-La and Hf-Bi, which gives the best results with the pseudopotential approximation. Hence, LanL2DZ basis set is a suitable basis set to optimize α-MoO_3 with pseudopotential approximation [37–39]. The HOMO-LUMO gap and density of states spectrum (DOS) of α-MoO_3 nanostructures are calculated using Gauss Sum 3.0 package [40]. The energy convergence is obtained within the range of 10–5 eV, during the optimization of α-MoO_3 nanostructures.

3. Results and discussion

The present work mainly focuses on the study of ionization potential (IP), HOMO-LUMO gap, dipole moment, electron affinity (EA), Mulliken population and adsorption properties of NH_3 gas molecules in MoO_3 base material with the incorporation of impurities such as Ti, Zr and F in α-MoO_3 nanostructures. The reason behind the selection of Ti, Zr and F as impurities is that Ti and Zr belong to the transition metals like Mo. The electronic and structural properties of α-MoO_3 nanostructure can be controlled and fine-tuned with chemical modifications, such as doping [41]. Especially, the doping methodology has been widely utilized for numerous conjugated polymers, while dopants play a vital role in modifying their electronic properties of conventional covalent semiconductors [42]. This doping technique can be performed either by application of an external electric field or charge transfer. Owing to the application of doping mechanism, optical and electronic properties of the respective conducting polymers can be widely engineered. In addition, the doping effect influences the transfer charge from semiconductor to metal or

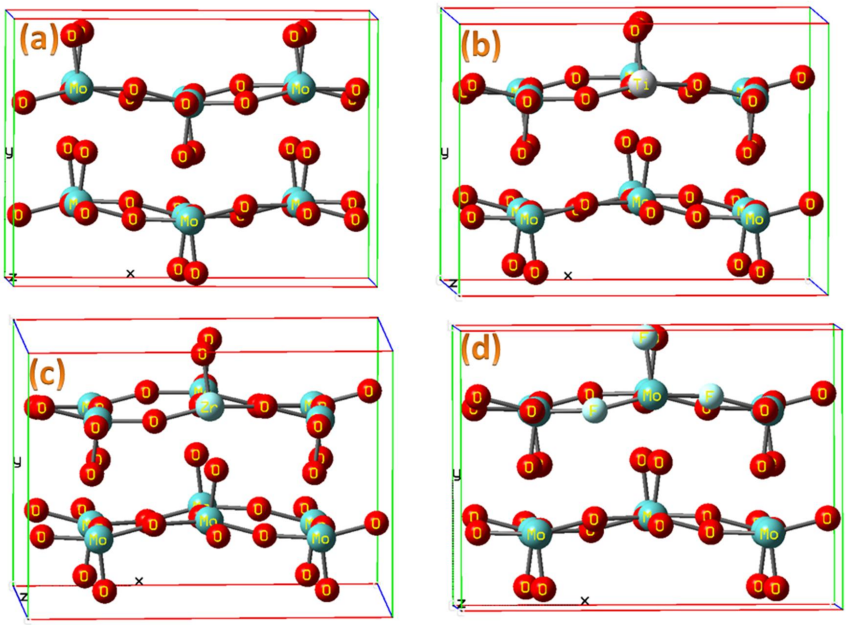

Figure 1. (Color online) (a) Pristine, (b) Ti substituted, (c) Zr substituted and (d) F substituted α-MoO_3 nanostructure.

insulator based on the concentration of a dopant [43]. The electronic properties of conjugated polymers can be easily fine-tuned either by atomic/molecular scale doping or chemical modification [41]. Kaloni et al. [44, 45] have reported the effect of the doping mechanism on polythiophene and polypyrrole based materials and studied the structural and electronic properties of pure and doped polymers. In the present work, α-MoO_3 nanostructures get distorted, while optimizing the base material with Ti, Zr and F elements as dopant, which results in the variation of electronic properties. Moreover, the conductivity of α-MoO_3 base material changes with the substitution of impurities. In addition, fluorine is abundant in electrons compared to oxygen, which leads to an increase in n-type behavior. Based on these aspects, the dopants are selected to incorporate in α-MoO_3 base material and these impurities tune the conducting property in α-MoO_3 base material. Therefore, the adsorption properties of NH_3 on α-MoO_3 nanostructures can be improved with the substitution impurities.

Figure 1 represents the structure of pristine, Ti, Zr and F substituted α-MoO_3 nanostructures, respectively. The structure of α-MoO_3 is taken from International Centre for Diffraction Data (ICDD) card number: 89-7112. The pristine α-MoO_3 nanostructure has twelve Mo atoms and thirty eight O atoms. Ti incorporated α-MoO_3 nanostructure has eleven Mo atoms, thirty eight O atoms and one Mo atom is replaced with one Ti atom. Similarly, Zr substituted α-MoO_3 nanostructure has eleven Mo atoms, thirty eight O atoms and one Mo atom is replaced with one Zr atom. In the case of F substituted α-MoO_3 nanostructure, it has twelve Mo atoms, thirty five O atoms and three O atoms are replaced with three F atoms for enhancing the adsorption properties of NH_3 on α-MoO_3 base material.

3.1. Structural stability and electronic properties of α-MoO_3 nanostructures

The structural stability of pristine, Ti, Zr and F substituted α-MoO_3 nanostructures can be described in terms of formation energy as shown in equation (3.1)

$$E_{\text{form}} = 1/n[E(\alpha\text{-MoO}_3 \text{ nanostructure}) - pE(\text{Mo}) - qE(\text{O}) - rE(\text{dopant})], \tag{3.1}$$

where $E(\alpha$-MoO_3 nanostructures) refers to the total energy of α-MoO_3 nanostructures, E(Mo), E(O) and E(dopant) represent the corresponding energy of isolated Mo, O and dopant atoms namely Ti, Zr

Table 1. Formation energy, dipole moment and point group of α-MoO_3 nanostructures.

Nanostructures	Formation energy (eV)	Dipole moment (D)	Point group
Pristine α-MoO_3 nanostructure	−4.38	5.62	C_1
Ti substituted α-MoO_3 nanostructure	−4.36	19.18	C_1
Zr substituted α-MoO_3 nanostructure	−4.30	35.08	C_1
F substituted α-MoO_3 nanostructure	−4.40	40.47	C_1

and F. p, q and r represent the total number of Mo, O and dopant atoms, respectively, and n is the total number of atoms in α-MoO_3 nanostructure. The dipole moment, point symmetry and the formation energy of pristine, Ti, Zr and F substituted α-MoO_3 nanostructures are tabulated in table 1. The formation energy of pristine, Ti, Zr and F substituted α-MoO_3 nanostructures is −4.38, −4.36, −4.30 and −4.40 eV, respectively.

Before studying the adsorption characteristics, the structural stability of α-MoO_3 base material must be studied. The structural stability of α-MoO_3 nanostructures slightly decreases with the substitution of Ti and Zr. The formation energy of Ti and Zr substituted α-MoO_3 nanostructures is relatively low compared to pristine α-MoO_3 nanostructures. By contrast, the stability of α-MoO_3 nanostructure slightly increases with the substitution of F. The dipole moment (DP) gives a clear picture about the distribution of charges in α-MoO_3 nanostructure. The corresponding dipole moment value of pristine, Ti, Zr and F incorporated α-MoO_3 nanostructures is 5.62, 19.18, 35.08 and 40.47 D. Low value of DP is recorded for pristine α-MoO_3 nanostructure. It infers that the charge distribution is almost uniform, but not in the case of impurity substituted α-MoO_3 nanostructures. Furthermore, C_1 point groups are observed for all α-MoO_3 nanostructures, which only exhibit identical operation.

The electronic properties of pristine, Ti, Zr and F incorporated α-MoO_3 nanostructures can be discussed in terms of the highest occupied molecular orbital (HOMO) and the lowest unoccupied molecular orbital (LUMO) [46, 47]. In the present work, the electronic properties and adsorption properties of NH_3 on α-MoO_3 nanostructures are studied for a small cluster. The HOMO-LUMO gap of pristine, Ti, Zr and F substituted α-MoO_3 nanostructures is 4.68, 2.03, 2.22 and 1.9 eV, respectively. The deviation in the HOMO-LUMO gap between experiment and theoretical values arises owing to the selection of the basis set [11]. Moreover, DFT method is broadly linked to the ground state. Thus, the exchange-correlation potential between the excited electronic states may be underestimated. The HOMO-LUMO gap of α-MoO_3 nanostructure decreases with the substitution of Ti, Zr and F. Thus, the electronic configuration of Mo, Zr, F and Ti element differs, the occupied states also differ. The corresponding electronic configuration of Ti, Zr and Mo is [1s2 2s2 2p6 3s2 3p6 3d2 4s2], [1s2 2s2 2p6 3s2 3p6 3d10 4s2 4p6 4d2 5s2] and [1s2 2s2 2p6 3s2 3p6 3d10 4s2 4p6 4d5 5s1]. In the case of Ti and Zr atom, the outermost s-orbital is completely filled with electrons and the electrons are partially occupied in d-orbital. Therefore, the s and d-states can be chosen as occupied and unoccupied state, respectively. Moreover, for Zr atom, the d-state is unfilled. In the case of Mo atom, the outermost s-orbital and d-orbital are not completely filled with electrons. Thus, due to the doping effects of Ti, Zr and F, the orbital overlapping leads to the variation in the energy gap in α-MoO_3 nanostructures. The HOMO-LUMO level and the energy gap of α-MoO_3 nanostructures are tabulated in table 2.

The density of states spectrum (DOS) gives an insight into the localization of charges in various energy intervals in α-MoO_3 nanostructures. The DOS spectrum and visualization of HOMO-LUMO gap of pristine, Ti, Zr and F substituted α-MoO_3 nanostructure are shown in figures 2–5, respectively. In the present work, the localization of charges is recorded to be more at LUMO level than at HOMO level, which is confirmed by more peak maxima at LUMO level. More peak maxima in α-MoO_3 nanostructures arise due to the orbital overlapping of Mo atoms and O atoms in α-MoO_3 base material. Moreover, the peak maxima in the virtual orbitals of α-MoO_3 base material are more favorable for adsorption characteristics, since the transfer of electrons between NH_3 molecules and virtual orbitals can take place easily.

Table 2. Adsorption energy, Mulliken population, HOMO-LUMO gap and average energy gap variation of α-MoO_3 nanostructures.

α-MoO_3 nanostructures	E_{ad}	Q (e)	E_{HOMO}	E_{FL} (eV)	E_{LUMO}	E_g (eV)	E_g^a (%)
Pristine α-MoO_3	–	–	−11.13	−8.79	−6.45	4.68	–
A	1.09	0.30	−11.04	−8.755	−6.47	4.57	2.41
B	−2.45	0.11	−11.04	−8.685	−6.33	4.71	0.64
C	−8.16	0.93	−8.55	−6.95	−5.35	3.2	46.25
D	−11.70	0.56	−9.13	−8.195	−7.26	1.87	150.27
Ti substituted α-MoO_3	–	–	−10.13	−9.115	−8.1	2.03	–
E	−0.27	0.19	−9.46	−8.785	−8.11	1.35	50.37
F	−2.72	0.10	−10.34	−9.275	−8.21	2.13	4.69
Zr substituted α-MoO_3	–	–	−10.48	−9.37	−8.26	2.22	–
G	−1.09	0.13	−10.15	−9.22	−8.29	1.86	19.35
H	−3.26	0.08	−10.37	−9.31	−8.25	2.12	4.72
F substituted α-MoO_3	–	–	−7.9	−6.95	−6	1.9	–
I	−14.42	1.14	−8.22	−6.865	−5.51	2.71	29.89
J	−9.52	0.67	−9.12	−7.385	−5.65	3.47	45.24

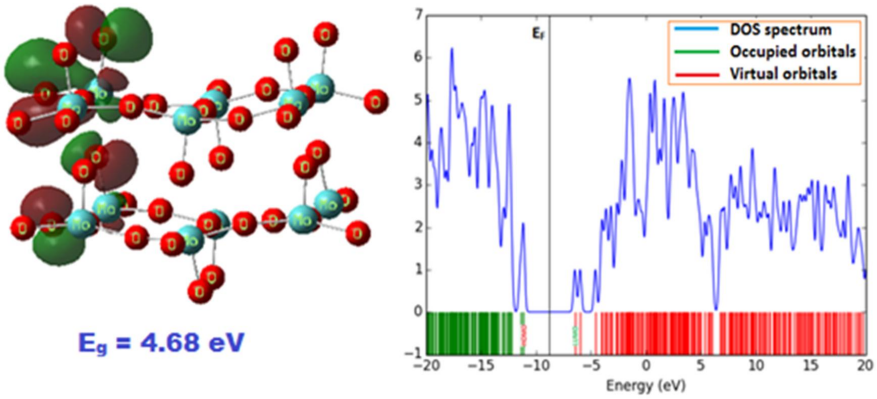

Figure 2. (Color online) HOMO-LUMO gap and density of states of pristine α-MoO_3 nanostructure.

The electronic properties of α-MoO_3 nanostructure can also be discussed with the ionization potential (IP) and electron affinity (EA) [48, 49]. Figure 6 represents the electron affinity and ionization potential of α-MoO_3 nanostructures. Generally, IP depicts the amount of energy required to remove the electron from α-MoO_3 nanostructures and the EA represents the energy change with the addition of electrons in α-MoO_3 nanostructures. The high value of ionization potential infers that the electrons are tightly bounded to the nucleus in α-MoO_3 nanostructure. Therefore, pristine, Ti and Zr substituted α-MoO_3 nanostructures have a high value of ionization potential, which infers that the electrons are strongly attracted to the nucleus and more energy is required to remove electrons from α-MoO_3 nanostructure. The low value of IP is recorded for F substituted α-MoO_3 nanostructure. Thus, less energy is required to remove an electron from F substituted α-MoO_3 nanostructure. Electron affinity plays an important role in plasma physics and in chemical sensors.

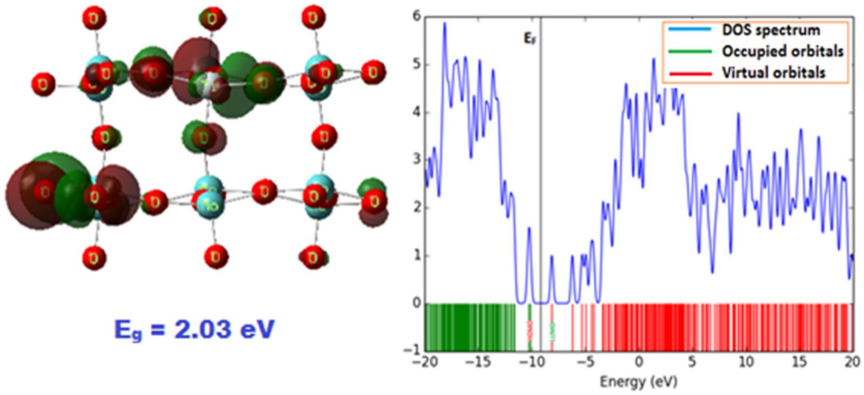

Figure 3. (Color online) HOMO-LUMO gap and density of states of Ti substituted α-MoO_3 nanostructure.

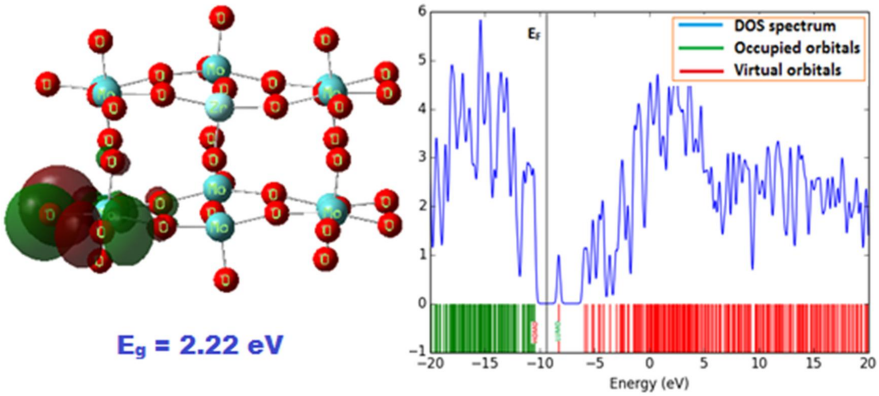

Figure 4. (Color online) HOMO-LUMO gap and density of states of Zr substituted α-MoO_3 nanostructure.

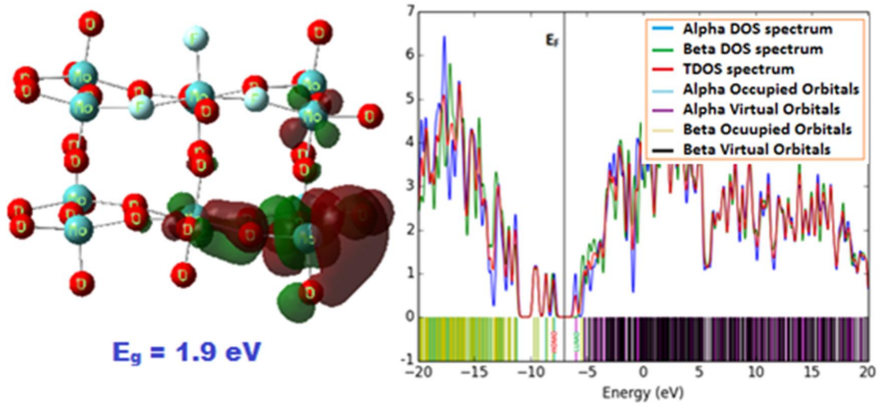

Figure 5. (Color online) HOMO-LUMO gap and density of states of F substituted α-MoO_3 nanostructure.

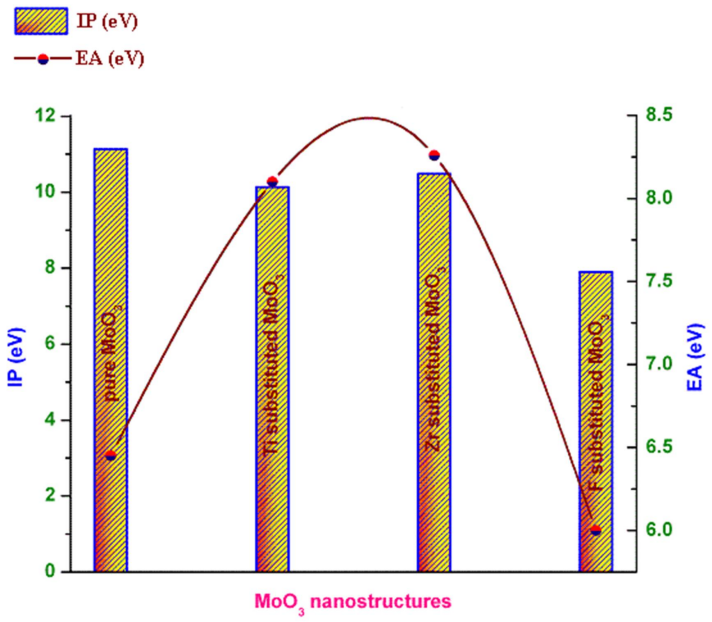

Figure 6. (Color online) IP and EA of α-MoO_3 nanostructure.

The EA value of pristine, Ti, Zr and F incorporated α-MoO_3 nanostructures is 6.45, 8.1, 8.26 and 6 eV, respectively, which is a favourable condition for chemical sensors. Usually, the amount of transfer of electrons depends on EA of the target gas molecule with the base material. Moreover, EA applies to the electronically conducting solid base material where it can be related to the position of Fermi energy level and the work function. If the base material has a high value of work function, it will in turn influence EA and it will act as electron acceptor and vice versa. Thus, the base material, which has low value of EA will partially transfer electrons between the target gas molecules and the conduction band of metal oxides. In the chemiresistor type of gas sensors, it is only due to the transfer of electrons that the change in the resistance is observed. However, in the present work EA for pristine and impurity substituted MoO_3 nanostructures, all have EA value of 6 to 8.26 eV. Furthermore, it can be suggested that MoO_3 nanostructures can be used as a chemical sensor.

3.2. Adsorption characteristics of NH_3 on α-MoO_3 nanostructures

Before studying the adsorption properties of NH_3 on MoO_3 nanostructures, NH_3 should be investigated in gas phase. The optimized bond length between nitrogen and hydrogen atom in NH_3 is 1.01 Å and the bond length between molybdenum and oxygen atoms in α-MoO_3 is 1.77 Å. These bond lengths are used during the optimization of α-MoO_3 nanostructures. Figure 7 refers to the adsorption of NH_3 gas molecule adsorbed on different sites, namely position A, B, C and D in pristine α-MoO_3 nanostructure. Figures 8–10 represent the adsorption of ammonia gas molecules adsorbed on various sites such as position E, F, G, H, I and J in Ti, Zr and F substituted α-MoO_3 nanostructure.

The adsorption energy of NH_3 gas molecules on α-MoO_3 nanostructure can be calculated by the equation (3.2) as follows:

$$E_{ad} = [E(MoO_3) + E(NH_3) - E(MoO_3/NH_3) + E(BSSE)], \tag{3.2}$$

where $E(MoO_3/NH_3)$ denotes the energy of MoO_3/NH_3 complex, $E(MoO_3)$ and $E(NH_3)$ are the isolated energies of MoO_3 and NH_3 molecules, respectively. The basis set superposition error (BSSE) [50] can be analyzed in terms of counterpoise technique to eliminate the overlap effects on basis functions. α-MoO_3 base material is found to have a negative value of energy which confirms the stability of the base

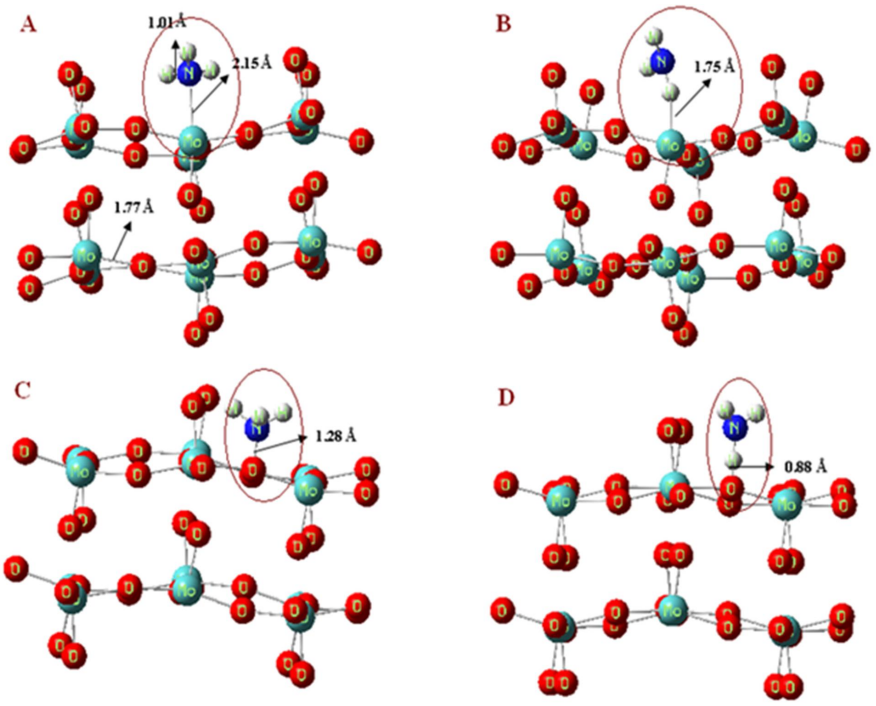

Figure 7. (Color online) NH_3 adsorbed on position A, B, C and D in pristine MoO_3 nanostructure.

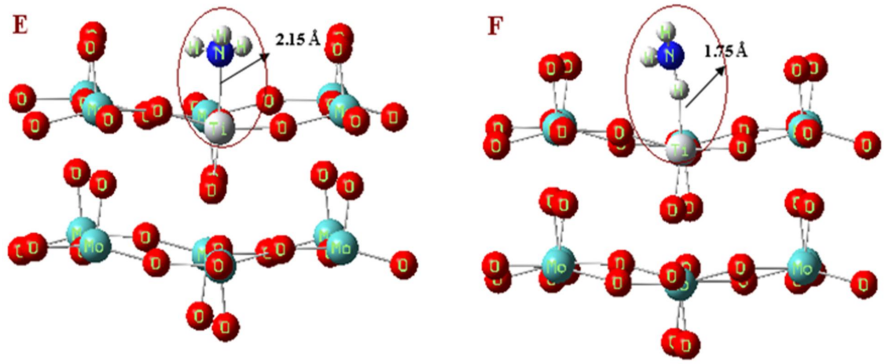

Figure 8. (Color online) NH_3 adsorbed on position E and F in Ti substituted MoO_3 nanostructure.

material. Moreover, when NH_3 gas molecules are adsorbed on α-MoO_3 nanostructures, negative values of the adsorption energy (E_{ad}) refer to the more stable system [51, 52].

In the present work, positions B to J all have negative values of adsorption energy. This infers that α-MoO_3 nanostructures are more stable and it is most suitable for gas sensor and as catalyst. The adsorption energies of pristine α-MoO_3 for positions A, B, C and D are 1.09, −2.45, −8.16 and −11.7 eV, respectively. The corresponding E_{ad} values of Ti incorporated α-MoO_3 for positions E and F are −0.27 and −2.72 eV. Zr substituted α-MoO_3 for positions G and H have E_{ad} values of −1.09 and −3.26 eV, respectively. F substituted α-MoO_3 for positions I and J has adsorption energy values of −14.42 and −9.52 eV, respectively. The other significant parameter to decide NH_3 adsorption characteristics is the band gap of α-MoO_3 nanostructure. Conductivity of α-MoO_3 nanostructure increases due to a decrease

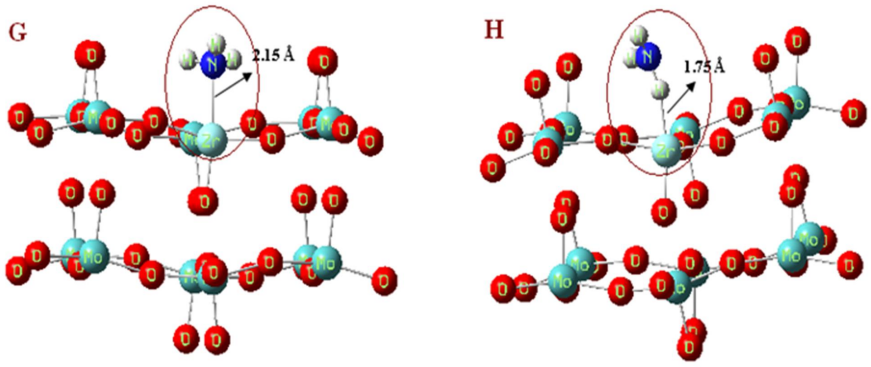

Figure 9. (Color online) NH_3 adsorbed on position G and H in Zr substituted MoO_3 nanostructure.

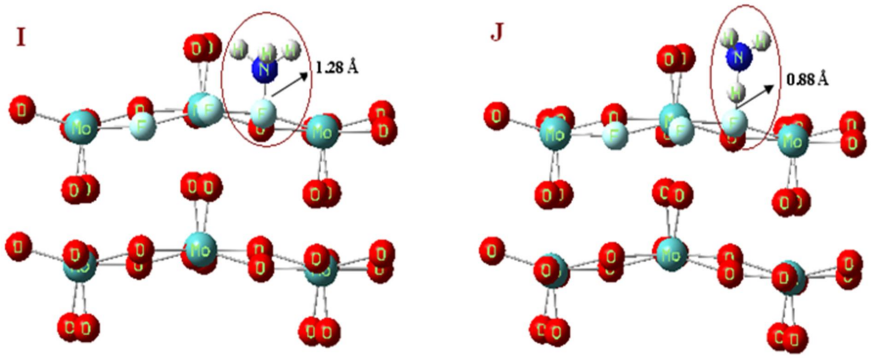

Figure 10. (Color online) NH_3 adsorbed on position I and J in F substituted MoO_3 nanostructure.

in the band gap, when NH_3 gets adsorbed on positions A, C, D, E, G and H of α-MoO_3 nanostructures, the corresponding band gap values are 4.57, 3.2, 1.87, 1.35, 1.86 and 2.12 eV, which are lower than their corresponding isolated counterpart. By contrast, conductivity of α-MoO_3 nanostructures decreases owing to an increase in the band gap, when NH_3 gets adsorbed on positions B, F, I and J with energy gap values of 4.71, 2.13, 2.71 and 3.47 eV, respectively, which are higher than their isolated counterpart. From the observations, it is revealed that the adsorption energy and the energy gap values change due to the adsorption of NH_3 in α-MoO_3 nanostructure.

Prasad et al. [53] reported the gas-sensing properties of MoO_3 with ammonia gas. Imawan et al. [19] proposed the gas-sensing properties of modified MoO_3 thin films using Ti-overlayers for NH_3 gas sensors. With the influence of Ti-overlayers in MoO_3 material, selectivity and sensitivity of NH_3 gas molecules get enhanced. The response of NH_3 mainly depends upon temperature. Furthermore, to improve the adsorption of NH_3 on MoO_3, the activation energy is required. The high operating temperature of molybdenum oxide enhances the catalytic activity. Therefore, the temperature dependent NH_3 gas sensitivity is possible in MoO_3 nanostructures. Based on the condition of the chemisorption mechanism, MoO_3 material shows good response to NH_3 gas molecules among other reducing gases such as H_2, CO and SO_2 at operating temperature of 200°C. Upon exposure of NH_3 gas molecules to molybdenum oxides, the resistance value changes leading to the detection of ammonia. The results obtained in the present work are for the ambient condition. Usually, by incorporating impurities or functionalization of the base material with Pd, Pt will decrease the operating temperature of metal oxide during gas sensing. Moreover, in the present study, the conductivity of α-MoO_3 material also varies

due to the transfer of electrons between NH_3 gas molecules and MoO_3 nanostructure. This validates the present work with the reported work.

In this work, the gas sensing properties of α-MoO_3 nanostructures are studied with the substitution of Ti, Zr and F impurities. From the observation, it is revealed that the pristine, Ti, Zr and F incorporated α-MoO_3 nanostructures are a promising material for sensing ammonia. The most favorable adsorption site of the NH_3 molecule on α-MoO_3 material can be concluded only after investigating the variation in the average energy gap (E_g^a) along with its respective isolated counterpart [54, 55]. Table 2 refers the HOMO-LUMO gap, percentage variation in energy gap, adsorption energy and Mulliken population. As a result, it is inferred that the most suitable site for adsorption of NH_3 molecules on α-MoO_3 nanostructures are positions C, D, E, G, I and J. The adsorption of N atom in NH_3 adsorbed on O, Ti, Zr and F atoms of pristine, Ti, Zr and F substituted α-MoO_3 nanostructure and the adsorption of H atom in NH_3 adsorbed on O and F atom of pristine and F substituted α-MoO_3 nanostructure are observed to be a more prominent adsorption site. The average energy gap variation is comparatively high among other adsorption sites.

The transfer of electrons between ammonia gas molecules and α-MoO_3 can also be analyzed with the help of Mulliken population analysis (Q) [56–58]. The negative charge of Mulliken population shows that the electrons are transferred from α-MoO_3 material to NH_3 gas molecules while the positive value of Q shows that the electrons are transferred from NH_3 gases to α-MoO_3 base material. In the present work, all positions have positive value of Q, which infers that the electrons are transferred from NH_3 molecules to α-MoO_3 nanostructure. The Q values of pristine α-MoO_3 nanostructure for positions A, B, C and D are 0.3, 0.11, 0.93 and 0.56 e, respectively. The corresponding Mulliken charge transfer values of Ti, Zr and F incorporated α-MoO_3 nanostructure for positions E, F, G, H, I and J are 0.19, 0.10, 0.13, 0.08, 1.14 and 0.67 e. As a result, it is observed that the high value of Mulliken charge transfer, average energy gap variation and adsorption energy are found to be more prominent for positions C, D, E, G, I and J. Conductivity of α-MoO_3 nanostructure for positions A, C, D, E, G and H increases owing to the narrowing of the energy gap. The remaining positions such as, B, F, I and J have less conductivity compared to the isolated counterpart. However, the conductivity decreases for positions I and J, the average energy gap variations are observed to be high, which is favorable for a good gas sensor. Therefore, the most favorable adsorption sites can be found only after investigating the adsorption energy, Mulliken population and HOMO-LUMO gap of α-MoO_3 nanostructure. Figures 11–20 represent the density of states spectrum and HOMO-LUMO gap of position A–J of α-MoO_3 nanostructures, respectively. Below the DOS spectrum, the green and red line indicates the HOMO-LUMO gap. From the DOS spectrum, it is clearly revealed that more peak maxima are observed in unoccupied orbital than in occupied orbital.

This implies that the electrons can easily transfer between α-MoO_3 and NH_3 gas molecules. Among all the optimum positions of α-MoO_3 nanostructure, positions C, D, E and J have more peak maximum in unoccupied orbital. Usually, in metal oxide based chemiresistors, which are used for gas/vapour sensing,

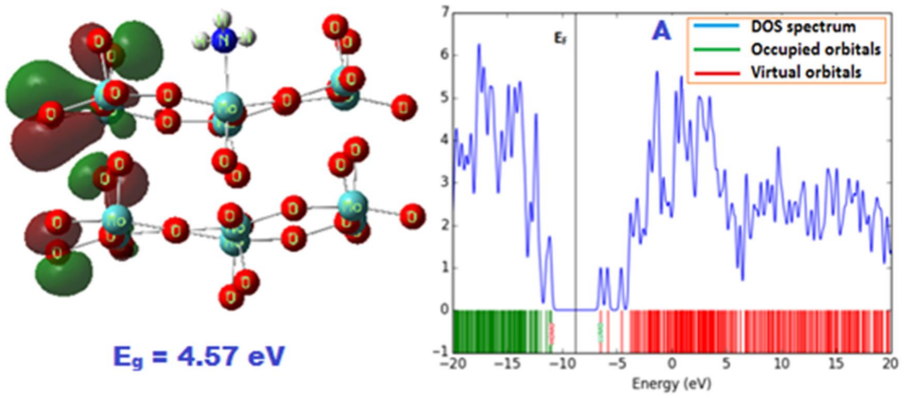

Figure 11. (Color online) HOMO-LUMO gap and density of states of position A.

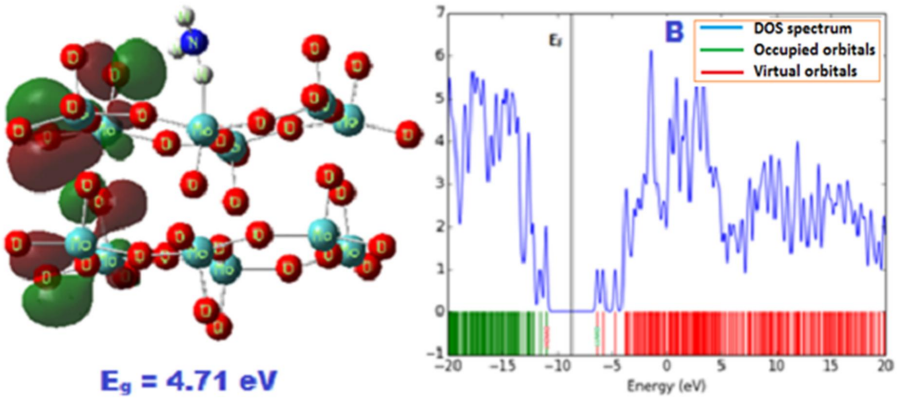

Figure 12. (Color online) HOMO-LUMO gap and density of states of position B.

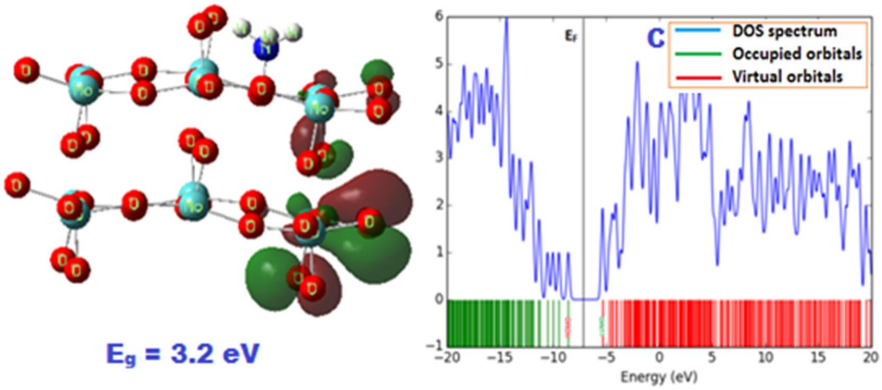

Figure 13. (Color online) HOMO-LUMO gap and density of states of position C.

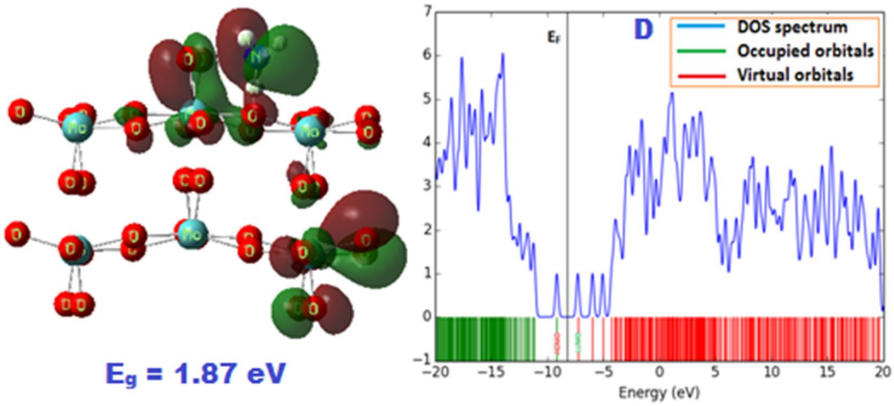

Figure 14. (Color online) HOMO-LUMO gap and density of states of position D.

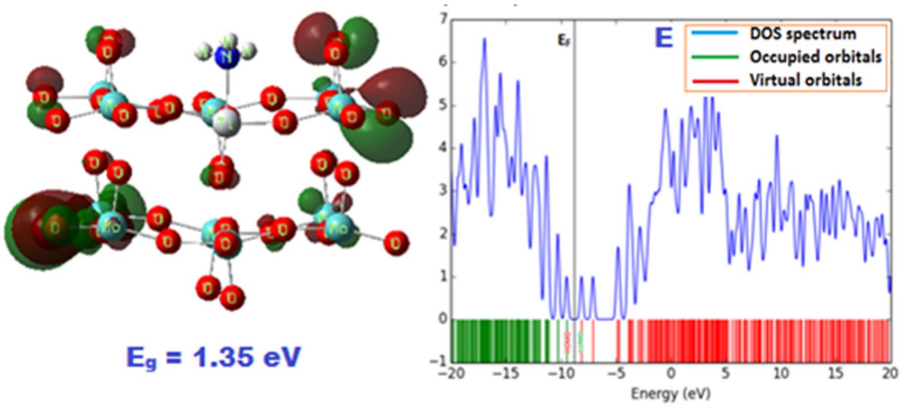

Figure 15. (Color online) HOMO-LUMO gap and density of states of position E.

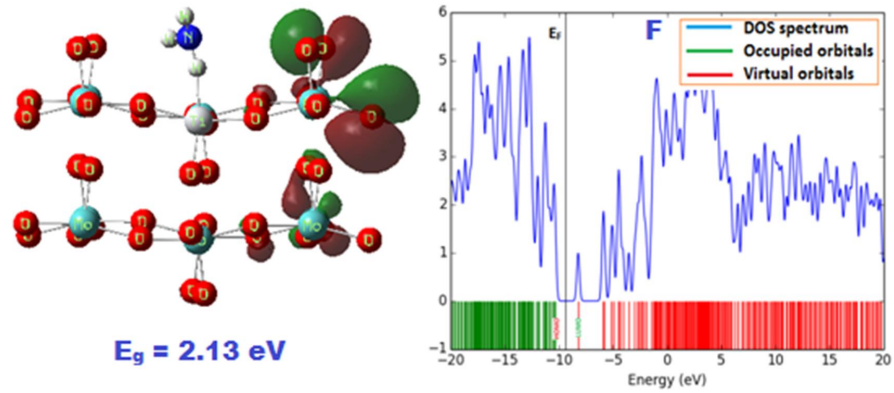

Figure 16. (Color online) HOMO-LUMO gap and density of states of position F.

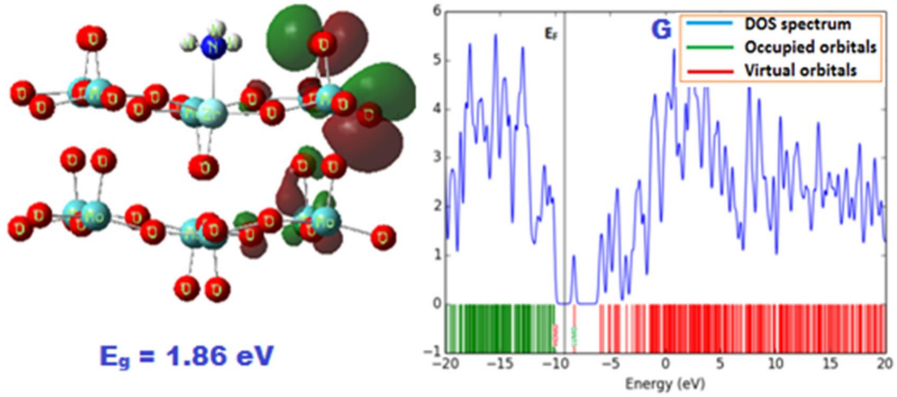

Figure 17. (Color online) HOMO-LUMO gap and density of states of position G.

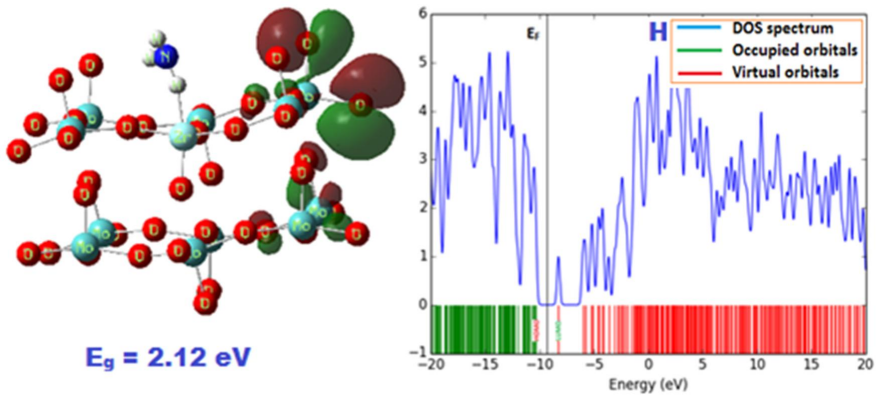

Figure 18. (Color online) HOMO-LUMO gap and density of states of position H.

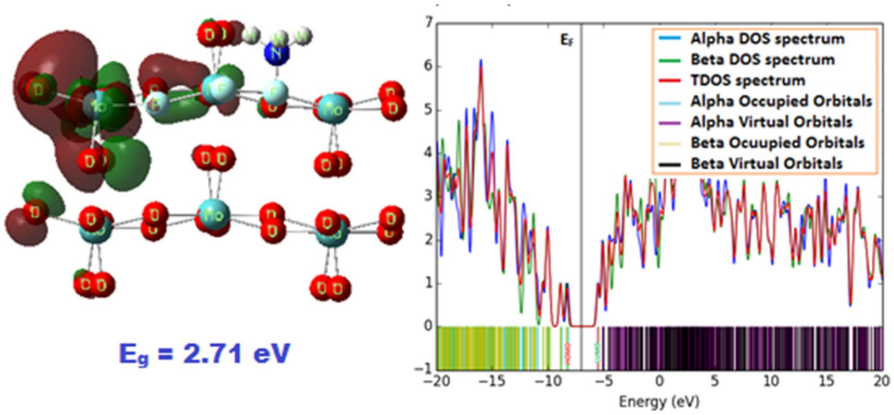

Figure 19. (Color online) HOMO-LUMO gap and density of states of position I.

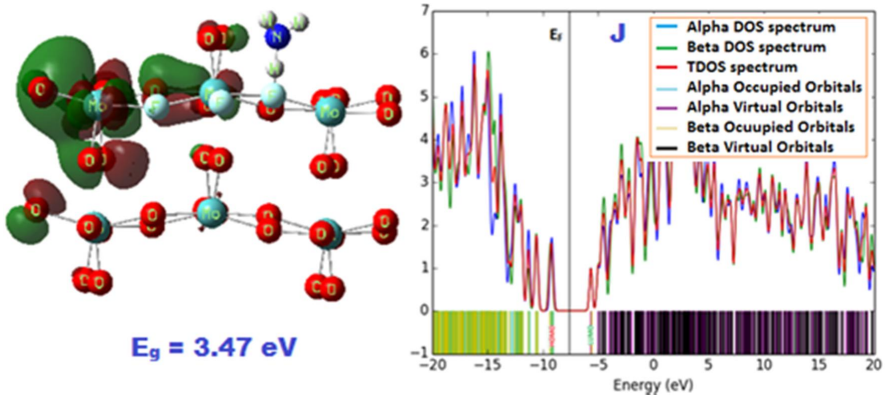

Figure 20. (Color online) HOMO-LUMO gap and density of states of position J.

the exchange of electrons takes place between the target gas and the base material. In the present study, a larger number of peak maxima is observed in the unoccupied orbital, which confirms the transfer of electrons between NH_3 target gas and α-MoO_3 base material for different positions (C, D, E and J). The alpha orbital and beta orbital exist for positions I and J, which arise due to spin up and down electrons due to orbital overlapping of F atoms with α-MoO_3 nanostructure. This further strengthens NH_3 adsorption properties on α-MoO_3 nanostructure, when substituted with F in α-MoO_3 base material. Hence, the variation of the band gap leads to the change in the resistance of α-MoO_3 nanostructure, which can be measured with a simple two probe arrangement. Analyzing all the aspects, it can be concluded that α-MoO_3 can be used as NH_3 gas sensing material in the mixed gas atmosphere.

4. Conclusions

To sum up, DFT method is employed to study NH_3 adsorption properties on α-MoO_3 material with B3LYP/LanL2DZ basis set. The electronic and structural stability of pristine, Ti, Zr and F substituted α-MoO_3 nanostructure has been investigated. The structural stability of all α-MoO_3 nanostructures has also been investigated using the formation energy. The electronic properties of α-MoO_3 nanostructures are discussed in terms of HOMO-LUMO gap, ionization potential and electron affinity. The dipole moment and the point group of pristine, Ti, Zr and F substituted α-MoO_3 nanostructures are also reported. The most prominent adsorption site of NH_3 on α-MoO_3 nanostructure is identified and discussed in terms of adsorption energy, average energy gap variation, Mulliken population analysis and HOMO-LUMO gap. Furthermore, the negative values of adsorption energy for the positions B to J confirm the stability of α-MoO_3 nanostructure upon adsorption of NH_3 molecules. The adsorption characteristics of NH_3 gas molecules get modified with the incorporation of Ti and F as impurities in α-MoO_3 base material. Moreover, there is no significant improvement in NH_3 adsorption properties on α-MoO_3 material with Zr substitution. In conclusion, the most favorable adsorption site of NH_3 on α-MoO_3 nanostructures is when the N atom in NH_3 adsorbed on O, Ti, Zr and F atoms of pristine, Ti, Zr and F substituted α-MoO_3 nanostructure and the adsorption of H atom in NH_3 adsorbed on the O and F atoms of pristine and F substituted α-MoO_3 nanostructure. Thus, α-MoO_3 nanostructure can be used as a good NH_3 gas sensor. In addition, the sensing characteristics of NH_3 can be modified with the incorporation of Ti and F as dopant in α-MoO_3 nanostructures.

References

1. Wei A., Wang Z., Pan L.-H., Li W.-W., Xiong L., Dong X.-Ch., Huang W., Chin. Phys. Lett., 2011, **28**, 080702, doi:10.1088/0256-307X/28/8/080702.
2. Stankova M., Vilanova X., Calderer J., Llobet E., Brezmes J., Gràcia I., Cané C., Correig X., Sens. Actuators B, 2006, **113**, 241, doi:10.1016/j.snb.2005.02.056.
3. Serebryakov D.V., Morozov I.V., Kosterev A.A., Letokhov V.S., Quantum Electron., 2010, **40**, 167, doi:10.1070/QE2010v040n02ABEH014147.
4. Sazhin S.G., Soborover E.I., Tokarev S.V., Russ. J. Nondestr. Test., 2003, **39**, 791, doi:10.1023/B:RUNT.0000020251.56686.a5.
5. Vidotti M., Dall'Antonia L.H., de Torresi S.I.C., Bergamaski K., Nart F.C., Anal. Chim. Acta, 2003, **489**, 207, doi:10.1016/S0003-2670(03)00757-8.
6. Chandiramouli R., Jeyaprakash B.G., Solid State Sci., 2013, **16**, 102, doi:10.1016/j.solidstatesciences.2012.10.017.
7. Chandiramouli R., Jeyaprakash B.G., RSC Adv., 2015, **5**, 43930, doi:10.1039/C5RA00734H.
8. Comini E., Faglia G., Sberveglieri G., Pan Z.W., Wang Z.L., Appl. Phys. Lett., 2002, **81**, 1869, doi:10.1063/1.1504867.
9. Comini E., Anal. Chim. Acta, 2006, **568**, 28, doi:10.1016/j.aca.2005.10.069.
10. Tomchenko A.A., Harmer G.P., Marquis B.T., Sens. Actuators B, 2005, **108**, 41, doi:10.1016/j.snb.2004.11.059.
11. Alizadeh S., Hassanzadeh-Tabrizi S.A., Ceram. Int., 2015, **41**, 10839, doi:10.1016/j.ceramint.2015.05.024.
12. Ferroni M., Guidi V., Martinelli G., Sacerdoti M., Nelli P., Sberveglieri G., Sens. Actuators B, 1998, **48**, 285, doi:10.1016/S0925-4005(98)00057-4.

13. Sunu S.S., Prabhu E., Jayaraman V., Gnanasekar K.I., Gnanasekaran T., Sens. Actuators B, 2003, **94**, 189, doi:10.1016/S0925-4005(03)00342-3.
14. Dadyburjor D.B., Jewur S.S., Ruckenstein E., Catal. Rev. Sci. Eng., 1979, **19**, 293, doi:10.1080/03602457908068057.
15. Larrubia M.A., Ramis G., Busca G., Appl. Catal. B, 2000, **27**, L145, doi:10.1016/S0926-3373(00)00150-8.
16. Sunu S.S., Prabhu E., Jayaraman V., Gnanasekar K.I., Seshagiri T.K., Gnanasekaran T., Sens. Actuators B, 2004, **101**, 161, doi:10.1016/j.snb.2004.02.048.
17. Imawan C., Steffes H., Solzbacher F., Obermeier E., Sens. Actuators B, 2001, **78**, 119, doi:10.1016/S0925-4005(01)00801-2.
18. Ferroni M., Guidi V., Martinelli G., Nelli P., Sacerdoti M., Sberveglieri G., Thin Solid Films, 1997, **307**, 148, doi:10.1016/S0040-6090(97)00279-4.
19. Imawan C., Solzbacher F., Steffes H., Obermeier E., Sens. Actuators B, 2000, **64**, 193, doi:10.1016/S0925-4005(99)00506-7.
20. Zhou J., Deng S.Z., Xu N.S., Chen J., She J.C., Appl. Phys. Lett., 2003, **83**, 2653, doi:10.1063/1.1613992.
21. Prasad A.K., Kubinski D.J., Gouma P.I., Sens. Actuators B, 2003, **93**, 25, doi:10.1016/S0925-4005(03)00336-8.
22. Patil R.S., Uplane M.D., Patil P.S., Appl. Surf. Sci., 2006, **252**, 8050, doi:10.1016/j.apsusc.2005.10.016.
23. Gesheva K.A., Ivanova T., Chem. Vap. Deposition, 2006, **12**, 231, doi:10.1002/cvde.200506404.
24. Ashraf S., Blackman C.S., Hyett G., Parkin I.P., J. Mater. Chem., 2006, **16**, 3575, doi:10.1039/b607335b.
25. Irmawati R., Shafizah M., Int. J. Basic Appl. Sci., 2009, **9**, 34.
26. Kannan B., Pandeeswari R., Jeyaprakash B.G., Ceram. Int., 2014, **40**, 5817, doi:10.1016/j.ceramint.2013.11.022.
27. Martínez H.M., Torres J., Rodríguez-García M.E., López Carreño L.D., Physica B, 2012, **407**, 3199, doi:10.1016/j.physb.2011.12.064.
28. Hussain O.M., Rao K.S., Mater. Chem. Phys., 2003, **80**, 638, doi:10.1016/S0254-0584(03)00101-9.
29. Nagarajan V., Chandiramouli R., Ceram. Int., 2014, **40**, 16147, doi:10.1016/j.ceramint.2014.07.046.
30. Nagarajan V., Chandiramouli R., J. Inorg. Organomet. Polym., 2014, **24**, 1038, doi:10.1007/s10904-014-0095-z.
31. Nagarajan V., Chandiramouli R., Superlattices Microstruct., 2015, **78**, 22, doi:10.1016/j.spmi.2014.11.027.
32. Frisch M.J., Trucks G.W., Schlegel H.B., Scuseria G.E., Robb M.A., Cheeseman J.R., Scalmani G., Barone V., Mennucci B., Petersson G.A., *et al.*, Gaussian 09, Revision D.01, Gaussian Inc., Wallingford CT, 2009.
33. Becke A.D., Phys. Rev. A, 1988, **38**, 3098, doi:10.1103/PhysRevA.38.3098.
34. Becke A.D., J. Chem. Phys., 1993, **98**, 1372, doi:10.1063/1.464304.
35. Hay P.J., Wadt W.R., J. Chem. Phys., 1985, **82**, 270, doi:10.1063/1.448799.
36. Wadt W.R., Hay P.J., J. Chem. Phys., 1985, **82**, 284, doi:10.1063/1.448800.
37. Chempath S., Zhang Y., Bell A.T., J. Phys. Chem. C, 2007, **111**, 1291, doi:10.1021/jp064741j.
38. Moberg D.R., Thibodeau T.J., Amar F.G., Frederick B.G., J. Phys. Chem. C, 2010, **114**, 13782, doi:10.1021/jp104421a.
39. Kadossov E.B., Soufiani A.R., Apblett A.W., Materer N.F., RSC Adv., 2015, **5**, 97755, doi:10.1039/C5RA08006A.
40. O'Boyle N.M., Tenderholt A.L., Langner K.M., J. Comput. Chem., 2008, **29**, 839, doi:10.1002/jcc.20823.
41. Roth S., Bleier H., Adv. Phys., 1987, **36**, 385, doi:10.1080/00018738700101032.
42. Deore B.A., Yu I., Freund M.S., J. Am. Chem. Soc., 2004, **126**, 52, doi:10.1021/ja038499v.
43. Heeger A.J., Kivelson S., Schrieffer J.R., Su W.P., Rev. Mod. Phys., 1988, **60**, 781, doi:10.1103/RevModPhys.60.781.
44. Kaloni T.P., Schreckenbach G., Freund M.S., Sci. Rep., 2016, **6**, 36554, doi:10.1038/srep36554.
45. Kaloni T.P., Schreckenbach G., Freund M.S., J. Phys. Chem. C, 2015, **119**, 3979, doi:10.1021/jp511396n.
46. Sriram S., Chandiramouli R., Jeyaprakash B.G., Struct. Chem., 2014, **25**, 389, doi:10.1007/s11224-013-0302-5.
47. Sriram S., Chandiramouli R., Balamurugan D., Thayumanvan A., Eur. Phys. J. Appl. Phys., 2013, **62**, 30101, doi:10.1051/epjap/2013130013.
48. Zhan C.-G., Nichols J.A., Dixon D.A., J. Phys. Chem. A, 2003, **107**, 4184, doi:10.1021/jp0225774.
49. Nagarajan V., Chandiramouli R., Alexandria Eng. J., 2014, **53**, 437, doi:10.1016/j.aej.2014.03.008.
50. Turi L., Dannenberg J., J. Phys. Chem., 1993, **97**, 2488, doi:10.1021/j100113a002.
51. Nagarajan V., Chandiramouli R., Struct. Chem., 2014, **25**, 1765, doi:10.1007/s11224-014-0451-1.
52. Nagarajan V., Chandiramouli R., J. Inorg. Organomet. Polym., 2015, **25**, 837, doi:10.1007/s10904-015-0167-8.
53. Prasad A.K., Gouma P.I., Kubinski D.J., Visser J.H., Soltis R.E., Schmitz P.J., Thin Solid Films, 2003, **436**, 46, doi:10.1016/S0040-6090(03)00524-8.
54. Nagarajan V., Chandiramouli R., Comput. Theor. Chem., 2014, **1049**, 20, doi:10.1016/j.comptc.2014.09.009.
55. Chandiramouli R., Srivastava A., Nagarajan V., Appl. Surf. Sci., 2015, **351**, 662, doi:10.1016/j.apsusc.2015.05.166.
56. Mulliken R.S., J. Chem. Phys., 1955, **23**, 1833, doi:10.1063/1.1740588.

57. Baei M.T., Peyghan A.A., Bagheri Z., Struct. Chem., 2013, **24**, 1099, doi:10.1007/s11224-012-0139-3.
58. Beheshtian J., Baei M.T., Bagheri Z., Peyghan A.A., Appl. Surf. Sci., 2013, **264**, 699, doi:10.1016/j.apsusc.2012.10.100.

Взаємодія газу NH_3 на наноструктурах α-MoO_3 — дослідження за допомогою теорії функціоналу густини

В. Нагараджан, Р. Чандірамулі

Школа електротехніки та електроніки, Академія мистецтв, наукових і технологічних досліджень Шанмуга (університет SASTRA), Танджавур, Таміл-Наду — 613 401, Індія

Структурна стійкість, електронні властивості і NH_3 адсорбційні властивості первинних, Ti, Zr і F заміщених α-MoO_3 наноструктур успішно вивчені, використовуючи теорію функціоналу густини з B3LYP/ LanL2DZ базисним набором. Структурна стійкість α-MoO_3 наноструктур обговорюється в термінах енергії утворювання. Електронні властивості первинних, Ti, Zr і F інкорпорованих α-MoO_3 наноструктур обговорюються в термінах HOMO-LUMO щілини, потенціалу іонізації та електронної афінності. α-MoO_3 наноструктури можуть бути точно-регульовані за допомогою підходящої домішки заміщення для покращення адсорбційних властивостей амоніяку, що може бути використано для виявлення NH_3 в змішаному середовищі. Дана робота дає розуміння про застосування α-MoO_3 наноструктур для виявлення NH_3.

Ключові слова: *наноструктура, адсорбція, NH_3, HOMO-LUMO щілина, MoO_3*